Autonomous motility of active filaments with nonlocal Stokesian hydrodynamics

Gayathri Jayaraman,[1] Sanoop Ramachandran,[2] Somdeb Ghose,[1]
M. Saad Bhamla,[2] P. B. Sunil Kumar,[2] and R. Adhikari[1]

[1] *The Institute of Mathematical Sciences, CIT Campus, Chennai 600113, India*
[2] *Department of Physics, Indian Institute of Technology Madras, Chennai 600036, India*

(Dated: April 10, 2012)

We simulate the nonlocal Stokesian hydrodynamics of an elastic filament with a permanent distribution of stresslets along its contour. A bending instability of an initially straight filament induces curvatures in the distribution of stresslets, thus producing a net hydrodynamic flow in which the filament propels autonomously. Depending on the ratio of stresslet strength to elasticity, the linear instability can develop into unsteady states with large-amplitude nonlinear deformations, where the filament conformation and the center of mass velocity fluctuate frequently. In planar flows, these unsteady states finally decay into steady states where the filament has constant translational or rotational motion. Our results can be tested in molecular-motor filament mixtures, synthetic chains of autocatalytic particles or other linearly connected systems where chemical energy is converted to mechanical energy in a fluid environment.

PACS numbers: 82.20.Wt, 87.16.A-, 47.63.M-

Components which convert chemical energy to mechanical energy internally are ubiquitous in biology. Common examples where this conversion leads to autonomous propulsion are molecular motors (at the subcellular level) and bacteria (at the cellular level) [1]. Recently, biomimetic elements which convert chemical energy into translational [2] or rotational [3] motion have been realized in the laboratory. While the detailed mechanisms leading to autonomous propulsion in these biological and soft matter systems shows a wonderful variety [4], their collective behavior tends to be universal and can be understood by appealing to symmetries and conservation laws [5]. This realization has led to many studies of the collective properties of suspensions of hydrodynamically interacting autonomously motile particles [6].

There are ample instances in biology, however, where the conversion of chemical to mechanical energy is not confined to a particle-like element but is, instead, distributed over a line-like element. Such a situation arises, for example, in a microtubule with a row of molecular motors converting energy while walking on it. The mechanical energy thus obtained not only produces motion of the motors but also generates reaction forces on the microtubule, which can deform elastically in response. Hydrodynamic interactions between the motors and between segments of the microtubule must be taken into account since both are surrounded by a fluid. This combination of elasticity, autonomous motility through energy conversion and hydrodynamics is found in biomimetic contexts as well. A recent example is provided by mixtures of motors which crosslink and walk on polymer bundles. A remarkable cilia-like beating phenomenon is observed in these systems [7]. A polymer in which the monomeric units are autocatalytic nanorods provides a nonbiological example of energy conversion on linear elastic elements. Though such elements are yet to be realized in the laboratory, active elements coupled to passive components through covalent bonds have been synthesized [2] and may lead to new kinds of nanomachines [3].

Motivated by these biological and biomimetic examples, we study, in this Letter, a semi-flexible elastic filament immersed in a viscous fluid with energy converting "active" elements distributed along its length. We present an equation of motion for the filament that incorporates the effects of nonlinear elastic deformation, active processes and nonlocal Stokesian hydrodynamic interactions. We use the lattice Boltzmann (LB) method to numerically solve the active filament equation of motion. Our simulations show that the distribution of active stresses induces a bending instability in a linear filament. These stresses, now distributed along a curved line, produce fluid flows that propel the filament. Depending on the ratio of activity and elasticity, the linear instability can develop into a nonlinear unsteady state with large-amplitude deformations where there are frequent changes in the filament conformation and its center of mass velocity. In planar flows, these unsteady states eventually decay into steady states where the filament translates ballistically or rotates steadily. In cubic flows, such steady states do not appear in the time scales of our simulation. We describe these results and our model in detail below.

Model: Our model for the active filament consists of N beads, with coordinates $\mathbf{r}_n$, interacting through a potential given by

$$U(\mathbf{r}_1,\ldots,\mathbf{r}_N) = \sum_{m=1}^{N-1} U_{\rm S}(\mathbf{b}_m) + \sum_{m=1}^{N-2} U_{\rm B}(\mathbf{b}_m,\mathbf{b}_{m+1}) + \frac{1}{2}\sum_{m,n=1}^{N} U_{\rm LJ}(\mathbf{r}_n-\mathbf{r}_m). \quad (1)$$

The two-body harmonic spring potential $U_{\rm S}(\mathbf{b}_m) = \frac{1}{2}k(b_m-b_0)^2$ penalizes departures of b_m, the modulus

of the bond vector $\mathbf{b}_m = |\mathbf{r}_m - \mathbf{r}_{m+1}|$, from its equilibrium value of b_0. The three-body bending potential $U_{\rm B}(\mathbf{b}_m, \mathbf{b}_{m+1}) = \bar{\kappa}(1 - \cos\phi_m)$ penalizes departures of the angle ϕ_m between consecutive bond vectors from its equilibrium value of zero. The rigidity parameter $\bar{\kappa}$ is related to the bending rigidity as $\kappa = b_0\bar{\kappa}$. The repulsive Lennard-Jones potential $U_{\rm LJ}$ vanishes if the distance between beads $r_{mn} = |\mathbf{r}_m - \mathbf{r}_n|$ exceeds $\sigma_{\rm LJ}$. The n-th bead experiences a force $\mathbf{f}_n = -\partial U/\partial \mathbf{r}_n$ when the filament stretches or bends from its equilibrium position. With the above choice of potential the connected beads approximate an inextensible, semi-flexible, self-avoiding filament.

Active non-equilibrium processes, such as those that convert chemical energy to mechanical energy, are internal to the fluid and hence cannot add net momentum to it. Then, the integral of the force density on a surface enclosing the active element must vanish. This is ensured if the active force density is the divergence of a stress. Since the active processes cannot add angular momentum to the fluid, the stress must be symmetric [8]. The most dominant Stokesian singularity with these properties is the stresslet [9]. There is a remaining freedom of the sign of the stresslet and its angle relative to the filament. Motivated by the tangential stresses exerted by motors walking on microtubules [7], we choose the stresslet to be extensile and oriented along the instantaneous tangent $\hat{\mathbf{t}}_n$ to the filament,

$$\boldsymbol{\sigma}_n = \sigma_0(\hat{\mathbf{t}}_n\hat{\mathbf{t}}_n - \mathbb{I}/d) \tag{2}$$

where d is the spatial dimension and $\sigma_0 > 0$ sets the scale of the activity. The results of other choices of sign and orientation will be presented elsewhere.

Elastic forces and active stresses produce velocities in the fluid. In the Stokesian regime, the velocity in a three-dimensional unbounded fluid at location $\mathbf{r}$ produced by a force $\mathbf{f}$ at the origin is $v_\alpha(\mathbf{r}) = O_{\alpha\beta}(\mathbf{r})f_\beta$ where $O_{\alpha\beta}(\mathbf{r}) = (\delta_{\alpha\beta} + \hat{r}_\alpha\hat{r}_\beta)/8\pi\eta r$ is the Oseen tensor, Cartesian directions are indicated by Greek indices, η is the fluid shear viscosity and $\hat{r}_\alpha = r_\alpha/r$. Similarly, the velocity at location $\mathbf{r}$ produced by a stresslet $\boldsymbol{\sigma}$ at the origin is $v_\alpha(\mathbf{r}) = D_{\alpha\beta\gamma}(\mathbf{r})\sigma_{\beta\gamma}$ where $D_{\alpha\beta\gamma}(\mathbf{r}) = (-\hat{r}_\alpha\delta_{\beta\gamma} + 3\hat{r}_\alpha\hat{r}_\beta\hat{r}_\gamma)/8\pi\eta r^2$ [10]. In the presence of rigid or periodic boundaries the tensors $\boldsymbol{O}$ and $\boldsymbol{D}$ must be replaced by the appropriate Green's functions of Stokes flow that vanish at the boundaries or have the periodicity of the domain [10]. Similarly, two-dimensional Green's functions must be used when studying the motion of filaments in planar flows [9]. The velocity of the n-th bead is obtained by summing the force and activity contributions from all beads, including itself, to the fluid velocity at its location. An isolated spherical bead with a force $\mathbf{f}$ acquires a velocity $\mu\,\mathbf{f}$ where μ is its mobility. By symmetry, an isolated spherical bead with a stresslet $\boldsymbol{\sigma}$ cannot acquire a velocity. This gives the following equation of motion for the active filament

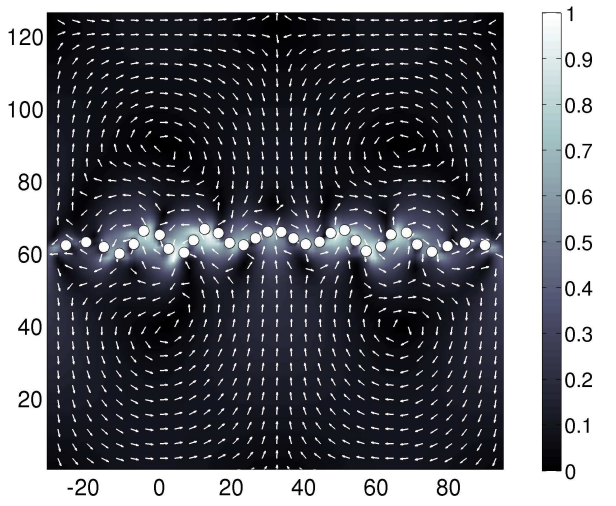

FIG. 1. (Color online) Bead positions (white circles) and fluid velocity field (arrows) after 4000 LB steps showing the linear instability of the filament. The background color shows the magnitude of fluid velocity at that point.

$$\dot{\mathbf{r}}_n = \sum_{m=1}^{N} [\mathbf{O}(\mathbf{r}_n - \mathbf{r}_m)\cdot\mathbf{f}_m + \mathbf{D}(\mathbf{r}_n - \mathbf{r}_m)\cdot\boldsymbol{\sigma}_m] \tag{3}$$

where $O_{\alpha\beta} = \mu\delta_{\alpha\beta}$ and $D_{\alpha\beta\gamma} = 0$ for $m = n$. Equations (1), (2) and (3) represent our model for the nonlocal Stokesian hydrodynamics of an active elastic filament. In the absence of bending rigidity and activity, our model reduces to Zimm dynamics of a polymer in a good solvent [11].

The ratio of the stresslet and Stokeslet terms in the equation of motion is a dimensionless measure of activity. Estimating the curvature elastic force as κ/L^2, where $L = Nb_0$ is the length of the filament, yields the "activity number" $\mathcal{A} = L\sigma_0/\kappa$. The rates of active and elastic relaxation are $\Gamma_\sigma = \sigma_0/\eta L^d$ and $\Gamma_\kappa = \kappa/\eta L^{d+1}$ respectively. Since $\mathcal{A} = \Gamma_\sigma/\Gamma_\kappa$ the activity number also measures the ratio of time scales associated with active and elastic relaxation. As $\mathcal{A} \to 0$ the active time scale diverges and conformational changes occur only due to elastic forces. As $\mathcal{A} \to \infty$ conformational changes due to activity are much more rapid than those due to elasticity.

Method: Here we use the lattice Boltzmann method [12] to obtain solutions to Eq. (3) in periodic planar and cubic geometries. The fluid is forced by the forces $\mathbf{f}_n$ and stresses $\boldsymbol{\sigma}_n$ through a standard method [13]. The resulting fluid velocity is interpolated to the position of the bead which is then updated using a forward Euler method. Forces and stresses corresponding to the updated conformation are calculated and passed on to the fluid and the velocity computation is repeated to advance

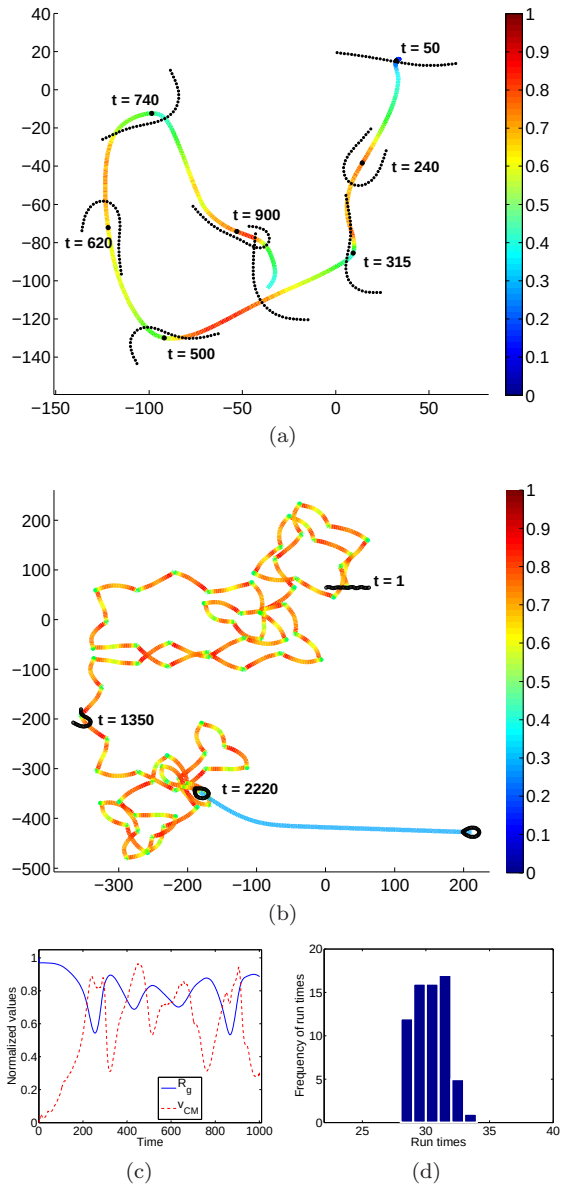

FIG. 2. (Color) (a) Filament motion for $\kappa = 0.1$ and $\sigma_0 = 0.01$, $\mathcal{A} = 6.4$ showing a run and tumble state. (b) Filament motion for $\kappa = 0.1$ and $\sigma_0 = 0.04$, $\mathcal{A} = 25.6$ showing frequent changes in conformation and changes in the center of mass velocity $v_{\rm CM}$. The filament ultimately reaches a ballistic steady state. In both (a) and (b) the color of the trace corresponds to $v_{\rm CM}$ normalized by its maximum value. (c) Time traces of the radius of gyration $R_{\rm g}$ normalized by its maximum value (solid blue curve) and the normalized $v_{\rm CM}$ (dashed red curve) corresponding to simulation in (a). (d) Distribution of run times of the filament corresponding to simulation in (b). Times are always in 10^3 LB steps.

to the next time step. All forces are kept small in lattice units to ensure that compressibilities and nonlinearities play a negligible role. The vorticity diffusion time scale L^2/η is kept smaller than all other time scales in the problem to ensure that the dynamics is Stokesian. We use lattice units in which both spatial and temporal discretization scales are unity. We choose $b_0 = 2$ and k such that there is less than 1% variation in contour length. We choose $\bar{\kappa}$ in the range 0.0 to 0.5 and σ_0 in the range 0 to 0.05, and N in the range 16 to 96. The initial filament conformation is a mixture of small amplitude transverse sinusoidal deformations of wavelengths that are a few integer multiples of L. The integration is carried out for several million time steps. Our results, unless otherwise stated, are for periodic planar lattices of size 128.

Results: We summarize our results in Figs. (1) - (3) and the movies in [14]. At early times, the filament develops a bending instability due to the activity. We show the nature of this instability, as $\mathcal{A} \to \infty$ and $k \to 0$, in Fig. (1) and its accompanying movie [14]. The extensile flow induced by the activity stretches the filament which then develops a sinusoidal instability that propagates inwards from the edges. The activity-induced linear instability proceeds unchecked due to the weakness of the elastic restoring forces. For $\mathcal{A} \to 0$ and $k \to \infty$, this instability is controlled by inextensibility and curvature to produce bent filament conformations. As the curvature develops, the flows produced by individual stresslets coherently add to form a net flow which propels the filament. Since the hydrodynamic drag on the filament is greater at its ends [15], a balance between elastic deformation, active propulsion and drag ensues and the filament propels steadily in a mildly deformed bow-shaped conformation, as shown in panel (a) of Fig. (3). We expect that, on dimensional grounds, the active filament will be linearly unstable only when $L > l_{\mathcal{A}} \sim \kappa/\sigma_0$, where numerical prefactors can be obtained from the linear stability analysis of Eq. (3). In contrast, the elastic Euler instability of a filament under force F occurs when $L > l_E \sim \sqrt{\kappa/F}$. A linear instability of passive filaments in an active medium, but without nonlocal hydrodynamics, was found in [16], while bow-shaped conformations, for filaments driven by external forces, were found in [17].

With increasing $\mathcal{A}$, the activity-induced linear instability cannot be contained by elastic restoring forces and the filament develops large-amplitude nonlinear deformations. An unsteady state is then produced, as shown in panel (b) of Fig. (3), where the filament undergoes conformational fluctuations as it autonomously propels. The flow acquires a rotational component of motion due to which there are frequent changes in direction of the center of mass velocity. This is shown in greater detail in Fig. 2(a) and its accompanying movie [14]. The radius of gyration and the center of mass velocity are anti-correlated, as is clear from Fig. 2(c). The conformations in this unsteady state depend sensitively on the initial conditions and on $\mathcal{A}$. The top panels of Fig. (3) show typical unsteady conformations for corresponding values of $\mathcal{A}$. For the largest values of activity in our simulations, the center of mass motion resembles a random walk, with short bursts of runs followed by frequent tum-

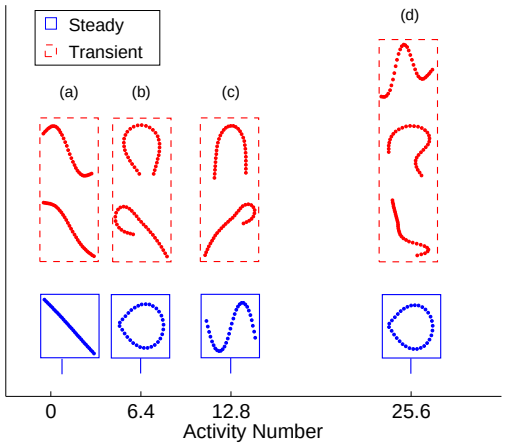

FIG. 3. (Color online) Filament conformations at various values of the activity number $\mathcal{A}$. Red dashed boxes correspond to transient conformations which evolve to the steady conformations below in blue solid boxes. Notches on the sides of the blue boxes indicate the corresponding value of $\mathcal{A}$.

bles, as seen in Fig. 2(b) and its accompanying movie [14]. The histogram of the run time distribution is decidedly non-Poissonian, as shown in Fig. 2(d), indicating that the steps of the walk may be correlated. It is remarkable that such "animate" behavior can be generated by Eq. (3).

The unsteady states described above decay into nonlinear steady states, where the filament is either ballistically propelling, panels (b) and (d) of Fig. (3), or steadily rotating, panel (c) of Fig. (3). In the ballistically propelling states, the filament resembles a teardrop. The transient unsteady state that decays to the ballistically propelling teardrop is shown in Fig. 2(b). The translational velocity is drastically reduced in the steady teardrop conformation, as seen in the accompanying movie [14]. Possible reasons for this could be the increased drag on the teardrop shape or the less effective addition of the stresslet velocities in that conformation. For intermediate values of $\mathcal{A}$, the filament assumes an S shape, and begins to rotate steadily as shown in the movie [14]. These elastically nonlinear and hydrodynamically nonlocal steady states cannot be obtained from a local, linear analysis of Eq. (3). In cubic flows, we see similar linear instabilities and unsteady states [14]. However, due to the large time scales ($\Gamma_\sigma^{-1} \sim 4 \times 10^6$ LB steps), we are unable to observe steady states for the duration of our simulations.

For a microtubule of size $L \sim 30\mu m$, $\kappa \sim 50pN\mu m^2$ with about 200 motors per micron exerting approximately $6pN$ of force, we obtain $\mathcal{A} \sim 60$. The activity can be manipulated in motor-polymer bundle systems or in polymers of autonomously motile nanorods over a large range of $\mathcal{A}$. These systems would be the best candidates for a verification of our results.

Discussion and conclusion: Our model has several important variations. We argued that active processes cannot add linear or angular momentum to the fluid and, so, must be represented by Stokesian singularities with those properties. This ruled out the Stokeslet and the rotlet but allowed for higher singularities, of which the stresslet, being the most dominant, was retained. The stresslet, with a $\boldsymbol{C}_\infty$ axis, is not forbidden by symmetry as a representation of a polar active element. If it is forbidden for non-symmetry reasons, we must use the potential dipole $\boldsymbol{d}$ [10], the leading singularity with polar symmetry, whose velocity field is $v_\alpha(\mathbf{r}) = G_{\alpha\beta}(\mathbf{r})d_\beta$, $G_{\alpha\beta} = (-\delta_{\alpha\beta}+3\hat{r}_\alpha\hat{r}_\beta)/8\pi\eta r^3$, in Eq. (3). The axis of the stresslet or the potential dipole can be oriented normally or obliquely to the local tangent of the filament and the stresslet can also be contractile, $\sigma_0 < 0$. The precise nature of the nonlinear steady states obtained from these various combination will be reported in future work. A generic equation of motion encompassing these specific cases is provided in [14].

Semi-flexibility is crucially important in obtaining the results above. A rigid rod ($\kappa = \infty$, $\mathcal{A} = 0$) will be immune to the active instability. Since the uniaxial axes of the stresslets and the rod are aligned, it cannot, by symmetry, acquire any translational or rotational motion. It is only by the breaking of this symmetry, possible when $\mathcal{A} \neq 0$, that the filament is able to acquire motion. The interplay between nonlocal hydrodynamics and semi-flexibility is necessary for the rotational motion of the filament, as has been noted earlier in a different context [17].

We have presented a model for an autonomously motile semi-flexible filament which takes into account nonlocal hydrodynamic interactions. It is surprising that a minimal model, such as ours, contains such rich phenomenology. Our model can be used to explore other remarkable effects of single active filaments like the cilia-like beating of motor-polymer bundles [7] as well as the collective properties of networks of active filaments, such as the cytoskeleton. Our model opens up the possibility of studying the non-equilibrium dynamics of active filaments including the effects of nonlinear elasticity and nonlocal hydrodynamics.

Financial support from PRISM, Department of Atomic Energy, Government of India (SG and RA) and computing resources through HPCE, IIT Madras is gratefully acknowledged.

Supplemental material: We present a generic model for autonomously motile elastic filaments which encompasses all the variations of Eq. (3). We include the potential dipole as a possible singularity that is polar. This is subdominant to the stresslet, but is the most important singularity if the stresslet vanishes due to non-symmetry reasons. In addition, we include an externally imposed

shear flow characterized by the shear rate tensor $\mathbf{E}$. We allow for any orientation of the stresslet axis $\hat{\mathbf{p}}_n$ and the potential dipole axis $\hat{\mathbf{d}}_n$ relative to the local tangent of the filament $\hat{\mathbf{t}}_n$. Thus, we have two new parameters in the model, $\theta_\sigma = \hat{\mathbf{p}}_n \cdot \hat{\mathbf{t}}_n$ and $\theta_d = \hat{\mathbf{d}}_n \cdot \hat{\mathbf{t}}_n$, the preferred angle that the stresslet and the potential dipole make with respect to the tangent. These angles can be made to vary along the filament, or may fluctuate in response to thermal noise. Finally, we include an external force $\mathbf{g}_n$ which may be due to externally imposed fields like gravity or electricity. Such fields are required when studying the driven motion, for example sedimentation under gravity, of active filaments. The generic equation of motion then, is

$$\dot{\mathbf{r}}_n = \sum_{m=1}^{N} [\mathbf{O}(\mathbf{r}_n - \mathbf{r}_m) \cdot \mathbf{f}_m + \mathbf{D}(\mathbf{r}_n - \mathbf{r}_m) \cdot \boldsymbol{\sigma}_m + \mathbf{G}(\mathbf{r}_n - \mathbf{r}_m) \cdot \mathbf{d}_m] + \mathbf{E} \cdot \mathbf{r}_n \tag{4}$$

$$\mathbf{f}_n = -\frac{\partial U}{\partial \mathbf{r}_n} + \mathbf{g}_n, \qquad \boldsymbol{\sigma}_n = \sigma_0(\hat{\mathbf{p}}_n\hat{\mathbf{p}}_n - \mathbb{I}/d), \qquad \mathbf{d}_n = d_0\hat{\mathbf{d}}_n. \tag{5}$$

$$O_{\alpha\beta}(\mathbf{r}) = \frac{1}{8\pi\eta r}(\delta_{\alpha\beta} + \hat{r}_\alpha\hat{r}_\beta),\ D_{\alpha\beta\gamma}(\mathbf{r}) = \frac{1}{8\pi\eta r^2}(-\hat{r}_\alpha\delta_{\beta\gamma} + 3\hat{r}_\alpha\hat{r}_\beta\hat{r}_\gamma),\ G_{\alpha\beta} = \frac{1}{8\pi\eta r^3}(-\delta_{\alpha\beta} + 3\hat{r}_\alpha\hat{r}_\beta) \tag{6}$$

For an unbounded two-dimensional fluid, the tensors can be obtained from their corresponding three-dimensional expressions through the replacements $1/r \to \log r$, $1/r^{n+1} \to 1/r^n$ for $n = 1, 2$ and $8\pi \to 4\pi$ [9]. For periodic flows, the forms given by Hasimoto must be used [18]. A principal advantage of the lattice Boltzmann method of solution is that the Green's functions above need not be computed explicitly. This is especially advantageous for complicated geometries where the Green's functions are typically not available in closed form. If required, the hydrodynamic interactions can be evaluated to higher orders in a multipole expansion [19] or can be formulated within the more rigorous framework of slender body theory [15].

The relaxation rates associated with elasticity, stresslet activity and potential dipole activity are $\Gamma_\kappa = \kappa/\eta L^{d+1}$, $\Gamma_\sigma = \sigma_0/\eta L^d$ and $\Gamma_d = d_0/\eta L^{d+1}$. The shear rate tensor introduces at least one additional independent relaxation rate $\Gamma_E = \dot{\gamma}$. The ratio of uniaxial and polar activities is $L\sigma_0/d_0$, indicating that uniaxial activity dominates for long filaments. This motivates why Eq. (3) retains only uniaxial activity. These equations form the basis by which we can explore the non-equilibrium dynamics of active filaments under external fields or externally imposed velocity gradients.

[1] F. J. Nédélec, T. Surrey, A. C. Maggs, and S. Leibler, Nature **389**, 305 (1997); S. Camazine, J. L. Deneubourg, N. R. Franks, J. Sneyd, G. Theraulaz, and E. Bonabeau, *Self-organization in Biological Systems* (Princeton University Press, New York, 2003).

[2] W. F. Paxton, K. C. Kistler, C. C. Olmeda, A. Sen, S. K. S. Angelo, Y. Cao, T. E. Mallouk, P. E. Lammert, and V. H. Crespi, J. Am. Chem. Soc. **126**, 13424 (2004); J. Vicario, R. Eelkema, W. R. Browne, A. Meetsma, R. M. La Crois, and B. L. Feringa, Chem. Commun. **31**, 3936 (2005).

[3] G. A. Ozin, I. Manners, S. Fournier-Bidoz, and A. Arsenault, Adv. Mater. **17**, 3011 (2005); J. M. Catchmark, S. Subramanian, and A. Sen, Small **1**, 202 (2005).

[4] J. G. Gibbs and Y. P. Zhao, Appl. Phys. Lett. **94**, 163104 (2009).

[5] R. A. Simha and S. Ramaswamy, Phys. Rev. Lett. **89**, 058101 (2002).

[6] L. H. Cisneros, R. Cortez, C. Dombrowski, R. E. Goldstein, and J. O. Kessler, Exp. Fluids **43**, 737 (2007); D. Saintillan and M. J. Shelley, Phys. Rev. Lett. **100**, 178103 (2008).

[7] T. Sanchez, D. Welch, D. Nicastro, and Z. Dogic, Science **333**, 456 (2011).

[8] J.-F. Joanny, private communication.

[9] A. T. Chwang and T. Y. Wu, J. Fluid Mech. **67**, 787 (1975).

[10] C. Pozrikidis, *Boundary Integral and Singularity Methods for Linearized Viscous Flow* (Cambridge University Press, Cambridge, 1992).

[11] M. Doi and S. F. Edwards, *The Theory of Polymer Dynamics* (Clarendon Press, Oxford, 1988).

[12] S. Succi, *The lattice Boltzmann equation for Fluid Dynamics and Beyond* (Clarendon Press, Oxford, 2001).

[13] R. W. Nash, R. Adhikari, and M. E. Cates, Phys. Rev. E **77**, 026709 (2008); R. W. Nash, R. Adhikari, J. Tailleur, and M. E. Cates, Phys. Rev. Lett. **104**, 258101 (2010).

[14] "See supplemental material at [url will be inserted by publisher] for a generic model of the autonomously motile filament and for movies of filament motion at different activity strengths for periodic planar and cubic geometries.".

[15] J. B. Keller and S. I. Rubinow,

J. Fluid Mech. **75**, 705 (1976).
[16] N. Kikuchi, A. Ehrlicher, D. Koch, J. A. Käs, S. Ramaswamy, and M. Rao, Proc. Natl. Acad. Sci. **106**, 19776 (2009).
[17] X. Xu and A. Nadim, Phys. Fluids **6**, 2889 (1994); M. C. Lagomarsino, I. Pagonabarraga, and C. P. Lowe, Phys. Rev. Lett. **94**, 148104 (2005).
[18] H. Hasimoto, J. Fluid Mech. **5**, 317 (1959).
[19] R. Kutteh, J. Chem. Phys. **119**, 9280 (2003).